The Astrophysical Journal, 705:1388–1394, 2009 November 10 doi:10.1088/0004-637X/705/2/1388

ADAPTIVE OPTICS ECHELLE SPECTROSCOPY OF [Fe II] 1.644 μm IN THE RW AUR JET: A NARROW SLICE DOWN THE AXIS OF THE FLOW

Patrick Hartigan[1] and Lynne Hillenbrand[2]
[1] Department of Physics and Astronomy, Rice University, 6100 S. Main, Houston, TX 77005-1892, USA
[2] Department of Astrophysics, California Institute of Technology, MC 105-24, Pasadena, CA 91125, USA
Received 2009 May 28; accepted 2009 September 22; published 2009 October 21

ABSTRACT

We present new adaptive optics echelle spectra of the near-infrared [Fe II] lines in the redshifted and blueshifted jets from the T Tauri star RW Aur. The spectra have an unprecedented combination of high spatial and spectral resolution that makes it possible to trace the dynamics of the flow to a projected distance of only 10 AU from the source. As noted by previous studies, the redshifted flow is much slower than its fainter blueshifted counterpart. Our observations clearly show that both the radial velocities and the emission line widths are larger closer to the source on both sides of the jet. The line widths are 20%–30% of the jet velocity on both sides of the flow, significantly larger than would be produced by a divergent constant velocity flow. The observed line widths could arise from a layered velocity structure in the jet or from magnetic waves. A bright knot in the redshifted jet has no concomitant increase in line width, implying that it is not heated by a bow shock. Alternate heating mechanisms include planar shocks, ambipolar diffusion, and magnetic reconnection.

Key words: ISM: Herbig–Haro objects – ISM: jets and outflows

1. INTRODUCTION

Stellar jets are an integral part of star formation during the first few million years when an accretion disk is present around young stars. How disks generate these highly collimated supersonic flows is a subject of much current observational and theoretical work. Most models drive jets magnetically from the rotating disk or from the point where the stellar field intersects the inner disk (e.g., Ferreira et al. 2006; Cai et al. 2008), and there is some evidence that magnetic fields are strong enough within a few hundred AU of the star to affect the flows (Ray et al. 1997; Hartigan et al. 2007). The location where the disk launches material into a jet varies between models, and observations are just now getting to the point where they can provide useful constraints on this process (see Ray et al. 2006, for a review).

The broad goal for observational work related to launching and collimating jets is to constrain the basic input parameters assumed by the models. Main outstanding questions involve understanding how disks accelerate material into jets, how jets become heated, and what role magnetic fields play in the flow dynamics. To answer these questions requires observations as close as possible to the star, because as the flow evolves, velocity variability in the jet creates internal bow shocks that dominate the heating and complicate the internal dynamics. If we wish to infer the shapes of streamlines and the location and strength of shock waves, and detect any rotational component to the outflow, we must measure precise radial velocities and resolve emission line widths down to the thermal broadening limit.

The observations described above are near or beyond the capabilities of existing facilities. The closest bright stellar jets are ∼140 pc away, so to study these systems on scales of 10 AU requires spatial resolutions $\lesssim 0\farcs1$. The strongest emission lines from jets are those in the optical ([S II], [N II], [O I], Hα, etc). However, in the optical, the required spatial resolution is available only from the *Hubble Space Telescope* (*HST*), and unfortunately current *HST* instrumentation delivers only moderate spectral resolution, which fails to reach the thermal broadening limit by a factor of 5 or more. The only atomic near-infrared lines of note in stellar jets are Fe [II] 1.644 μm and 1.667 μm. Ground-based adaptive optics systems on large telescopes reach the required spatial resolution and possess instruments that also deliver the necessary spectral resolution to study these lines in a few of the brightest jets. It is also becoming possible to study molecular jets close to their sources using radio interferometric observations of SiO (e.g., Cabrit et al. 2007; Codella et al. 2007).

Because it is bright, relatively close (∼140 pc), and visible all the way to the star, the RW Aur jet is one of the best targets in the sky to study how accretion disks launch jets. RW Aur was discovered as a variable star a little over a century ago (Ceraski 1906), and is well-known as having a rich emission line spectrum in the optical characteristic of a high accretion rate classical T Tauri star (Joy 1945; Hartigan et al. 1991; Stout-Batalha et al. 2000). The system is also a binary, with a companion located ∼ $1\farcs4$ from the primary (Joy 1945; White & Ghez 2001). The jet has both redshifted and blueshifted components, with the redshifted part having higher radial velocity (Hirth et al. 1994; Hamaan 1994). The jet and its bow shocks extend from the star for at least $100''$ (McGroarty & Ray 2004), and proper motions show the jet to be inclined 46° from the line of sight (López-Martín et al. 2003).

Several studies of RW Aur have focused on the properties of its jet on subarcsecond scales as it emerges from the source. High-resolution optical images of [O I] and [S II] traced the jet to within ∼0.3 arcsec, of the star (Dougados et al. 2000), and showed that it has a roughly constant opening angle of $3\fdg9$. The jet does not project back to a point at the star, indicating that the opening angle is wider within 30 AU of the source. Spectra of the jet from the Space Telescope Imaging Spectrograph (STIS) on the *HST* show that the density declines with distance from the star as the jet expands, and that the velocity asymmetry between the redshifted and blueshifted jets has increased over the last decade (Woitas et al. 2002). Emission-line spectroastrometry provides evidence for outflows on AU scales (Whelan et al. 2004), and the variability of high-velocity components of semiforbidden UV lines also implies a wind close

to the star (Gomez de Castro & Verdugo 2003), consistent with recent models of the Balmer line profiles (Alencar et al. 2005).

An intriguing observation of asymmetry in the velocity structure of the jet has been interpreted as evidence for rotation (Coffey et al. 2004; Woitas et al. 2005). However, these observations are controversial because the modest spectral resolution of STIS (55 km s^{-1}) makes it very difficult to infer rotational velocities of only a few km s^{-1}, and in the case of RW Aur the molecular disk rotates in the opposite sense of the inferred jet rotation (Cabrit et al. 2005). Precession can also mimic rotation signatures in outflows (Cerqueira et al. 2006).

Two high spectral resolution studies of the infrared [Fe II] lines in RW Aur have been done. Davis et al. (2003) used an echelle with 19 km s^{-1} resolution and a wide slit without adaptive optics to resolve the line widths in the redshifted and blueshifted jets. More recently, Pyo et al. (2006) used adaptive optics with the Subaru telescope with 0.″2 resolution, a 0.″3 wide slit, and 30 km s^{-1} velocity resolution to study the kinematics of the jet down to ∼30 AU from the source. Such observations provide important constraints on models of jet collimation and energetics.

In this paper, we present the first high resolution adaptive optics observations of a stellar jet taken with the near-IR spectrometer on Keck. These observations represent a significant improvement in the spatial and spectral resolution over previous studies—a factor of ∼3 better spectral resolution and 20% better spatial resolution than the *HST* STIS data, and a factor of 1.5 and 3 better spectral and spatial resolution, respectively, than the Subaru spectra. In addition, the slit width of 0.″068 is ∼4 times narrower than that of the Subaru spectra, so we can isolate a slim cross section of the jet. Both the spatial and spectral dimensions are subsampled a factor of ∼4 better than those of STIS, which enables more precise subtraction of the stellar point-spread function (PSF) close to the star.

The cost to pay for such high spatial and spectral resolution and a very narrow slit is a reduction in flux. We were unable to detect the fainter extended emission away from the axis of the RW Aur jet, and thus cannot address issues related to rotation. However, our observations clearly resolve the line widths and velocities in the jet for the first time to within 10 AU of the star. The narrow slit provides a sharp "cut" down the axis of the flow which is easy to interpret, and makes it possible to measure the geometry of the streamlines as the jet emerges from the disk.

2. OBSERVATIONS

We obtained spectra of the RW Aur jet with the NIRSPEC spectrograph and adaptive optics system attached to the W. M. Keck II telescope on Mauna Kea on 2006 December 17 UT. The position angle of the slit was 125° (along the axis of the jet), and the AO system used the target, RW Aur, as a natural guide star (R magnitude ∼ 10). The slit width was 68 mas, which projects to a distance of only 9.5 AU at the distance to the object of 140 pc, so these observations represent narrow slices down the axis of the flow.

Spectra include seven orders from 1.51 μm through 1.74 μm, with gaps of ∼0.03 μm where the spectra extend beyond the 1024 × 1024 InSb chip. The dispersion was 0.238 Å (4.34 km s^{-1}) per pixel at the wavelength of the [Fe II] 1.644 μm emission line. The velocity resolution of the instrument, defined by the FWHM of several OH night sky emission lines, was 20.3 km s^{-1} and remained constant throughout the night. The dispersion is about five times finer and the resolution about three times better than optical spectra of RW Aur obtained with the STIS on the *HST* (Woitas et al. 2002, 2005).

Wavelength shifts were less than 0.1 pixel between different sky spectra, so a single wavelength solution suffices for all spectra. We determined the wavelength scale from positions of OH emission lines in our night sky spectra (Rousselot et al. 1999), and from Kr and Ar lines in calibration lamp spectra. The number of lines per order is sparse, so uncertainties in the wavelength solutions are rather large, ∼± 5 km s^{-1} for 1σ. The wavelength calibration is most uncertain at the edges of orders. This uncertainty affects the velocity zero point of our spectra but has a negligible effect on the line profile shape or the velocity dispersion.

Flat fields taken with the continuum lamp showed an irregular interference pattern that introduced spurious patterns to our data. The chip is quite flat, with variations in pixel-to-pixel sensitivity only 1%–2%, so in lieu of a continuum flat we used the dithers of the multiple exposures along the slit to remove pixel-to-pixel variations. The PSF is well sampled both spatially and spectrally, further reducing the need for continuum flats.

Individual exposure times were 5 minutes in length. We initially acquired spectra in a grid centered on the RW Aur jet with offsets perpendicular to the axis of the jet at distances that ranged from −0.″204 to +0.″204, spaced in intervals of one slit width, 0.″068. However, observations with offsets from the axis ⩾ 0.1 arcsec showed no signal from [Fe II] so we resampled the interior part of the grid with 0.″034 spacings, and concentrated most of our spectra within ±0.1 arcsec of the axis. In all, 27 exposures had some [Fe II] signal. Nine additional spectra of blank sky taken throughout the night aided the wavelength calibration and background subtraction of OH night sky lines.

In practice, small spatial offsets exist between the desired and actual slit positions. Fortunately, these are easy to quantify with the 256 × 256 HgCdTe slit camera (SCAM) images, which are taken simultaneously with the spectra. RW Aur and RW Aur/c appear on all SCAM images, and define the SCAM plate scale to be 16.3 mas per pixel, close to the value quoted by Hornstein et al. (2002). The slit is visible on the SCAM images, and is 2.″20 in length. On the science camera, spectral images of the slit in the night sky emission lines subtend 118 pixels, so the plate scale of the longslit spectra is 18.6 mas per pixel.

Conditions were non-photometric, but SCAM images of RW Aur/c show the AO system produced stellar images with FWHM of 60 ± 13 mas at H throughout the night (Table 1). This spatial resolution is about 20% better than that obtained with optical diffraction-limited dithered *HST* slitless images of the HH 30 jet with the STIS (Hartigan et al. 2004), and a factor of 3 better than the Subaru spectra of Pyo et al. (2006). While some previous observations have suggested that the companion may also be a binary, our observations show only a single star, in agreement with White & Ghez (2001).

We combined the [Fe II] spectra into five position–velocity diagrams as described in Table 1 and Figure 1, using the position of RW Aur/c in the SCAM images to define where the slit was positioned during each exposure. The SCAM images also show that there were shifts of up to 0.10 arcsec along the slit, which we removed before averaging individual frames into the five output spectra, denoted 0.083-NE, 0.033-NE, Center, 0.047-SW, and 0.089-SW. After subtracting a background sky image from each object and removing any remaining hot pixels, we extracted the order of interest and corrected the spectra for tilts in the x- and y-directions using the observed trace of the RW Aur spectrum and the position of the night sky lines, respectively. The reduced

Table 1
Positional Offsets of RW Aur Slit Spectra

Sequence Number	Spatial Offset[a]	FWHM of PSF[b]	Output Image[c]
64	−0.099	0.065	0.083 NE
39	−0.093	0.064	
59	−0.078	0.042	
26	−0.062	0.083	
65	−0.044	0.052	0.033 NE
33	−0.039	0.080	
75	−0.024	0.049	
76	−0.024	0.049	
77	−0.024	0.049	
50	−0.008	0.049	Center
51	−0.008	0.049	
52	−0.008	0.049	
53	−0.008	0.049	
82	−0.008	0.046	
55	0.000	0.072	
56	0.000	0.072	
57	0.000	0.072	
58	0.000	0.072	
30	0.003	0.088	
66	0.029	0.054	
78	0.044	0.046	0.047 SW
79	0.044	0.046	
80	0.044	0.046	
35	0.057	0.070	
22	0.085	0.073	0.089 SW
72	0.086	0.051	
67	0.096	0.070	

Notes.
[a] Spatial offset perpendicular to the axis of the jet. Positive values denote offsets to the SW, and negative values are offsets to the NE. The position angle of the slit on the sky was 125 degrees.
[b] FWHM in arcseconds of the SCAM image of RW Aur/c.
[c] Each spectrum was averaged into one of five output images.

data have spatial position along the *y*-axis and heliocentric radial velocity along the *x*-axis. The heliocentric radial velocity of RW Aur is 14 ± 5 km s^{-1} (Hartmann et al 1986).

3. ANALYSIS AND RESULTS

The method we use to extract extended emission lines from longslit spectra is that of Hartigan et al. (2004). Briefly, the spatial PSF of the star is defined by co-adding the counts in a wavelength region on either side of the emission line, and the PSF is interpolated linearly between these regions. Once one obtains a spectrum at the location of the star, multiplying this spectrum by the spatial PSF and subtracting it from the image leaves only the extended line emission. To obtain a stellar spectrum we split the spectrum into redshifted and blueshifted portions. The blueshifted flow occurs to the SE, so for the blueshifted portion of the spectrum we extracted the stellar spectrum from the NW part of the stellar PSF. Similarly, the SE part of the PSF defined the spectrum of the redshifted portion of the spectrum. Combining the two halves gives a position–velocity diagram for the extended line emission. The procedure is implemented through an imfort program in IRAF.[3]

[3] IRAF is distributed by the National Optical Astronomy Observatories, which is operated by the Association of Universities for Research in Astronomy (AURA) under cooperative agreement with the National Science Foundation.

Figure 1 shows that the position–velocity diagrams of the five positions are essentially identical. We could not detect any flux at distances greater than 0.1 arcsec away from the axis of the flow. Combining the AO-corrected FWHM of 60 mas in quadrature with the slit width of 68 mas we obtain ∼90 mas for the expected spatial extent of an unresolved source. Hence, our observations do not clearly resolve the spatial width of the jet. *HST*–STIS spectra of [S II] with comparable spatial resolution to our spectra do resolve the jet spatially (Woitas et al. 2002), but with a much lower spectral resolution.

We measured the radial velocities and FWHM from each 5-minute exposure individually and combined the results to produce each point and error bar in Figure 2 and Figure 3. The velocity of the redshifted flow is almost a factor of 2 lower than that of the blueshifted flow, as observed already by Pyo et al. (2006), and by Hirth et al. (1994). The combination of exquisite spatial and spectral resolution of the Keck AO system reveals that the radial velocity of the redshifted [Fe II] decreases in the first 0.″2, and then stays constant. The redshifted emission is slower, brighter, and more peaked in velocity than the blueshifted emission.

Figure 3 shows that the [Fe II] line is well-resolved spectrally, and its width increases monotonically in both the jet and the counterjet as the distance to the source decreases. The blueshifted flow has a line width about 50% larger than its redshifted counterpart. The larger line width of the blueshifted flow was noted before by Pyo et al. (2006), though that work did not have sufficient spatial and spectral resolution to detect the rise of line width within ∼30 AU of the source within the redshifted jet.

RW Aur has many permitted emission lines in its spectrum (Petrov et al. 2001), and several of the Brackett lines appear in our observations. A good way to determine whether or not these lines have a wind component is to perform spectroastrometry, which determines spatial offsets of the emission lines with respect to the adjacent continuum (e.g., Ray et al. 2006). While the method is powerful because it is very sensitive to small positional shifts and can be done as a function of velocity for resolved emission lines, it suffers from the important limitation that the weighted average of the line emission at a given velocity determines the amount of the spatial shift. Hence, if, for example, a blueshifted part of the line profile has a centroid shifted 2 AU from the star, there need not be any emission at 2 AU. Such a shift only implies that the weighted average of the emission from the star and in the flow is offset from the stellar position by 2 AU at that radial velocity.

Figure 4 presents spectroastrometry in the vicinity of the bright Brackett and [Fe II] lines. The spectra show no indications of any wind signatures in Br-12 or Br-11 at the 0.04 pixel level (∼ 0.1 AU). However, both the [Fe II] 1.644 μm line and the much weaker [Fe II] 1.677 μm line exhibit clear redshifted and blueshifted astrometric signatures even though the line emission is dominated by photospheric and veiling flux at this wavelength.

4. DISCUSSION

Ferreira et al. (2006) summarize three proposed geometries for magnetohydrodynamic jets in which open field lines are anchored to rotating young stellar objects. The models are all variations of the magnetocentrifugal mechanism (Blandford & Payne 1982), but differ in their mass loading: the disk wind model Königl & Pudritz (2000) typically loads material over a wide range of radii; the X-wind model (Shang et al. 2002) drives the wind from a narrow range of radii; and the hybrid stellar wind

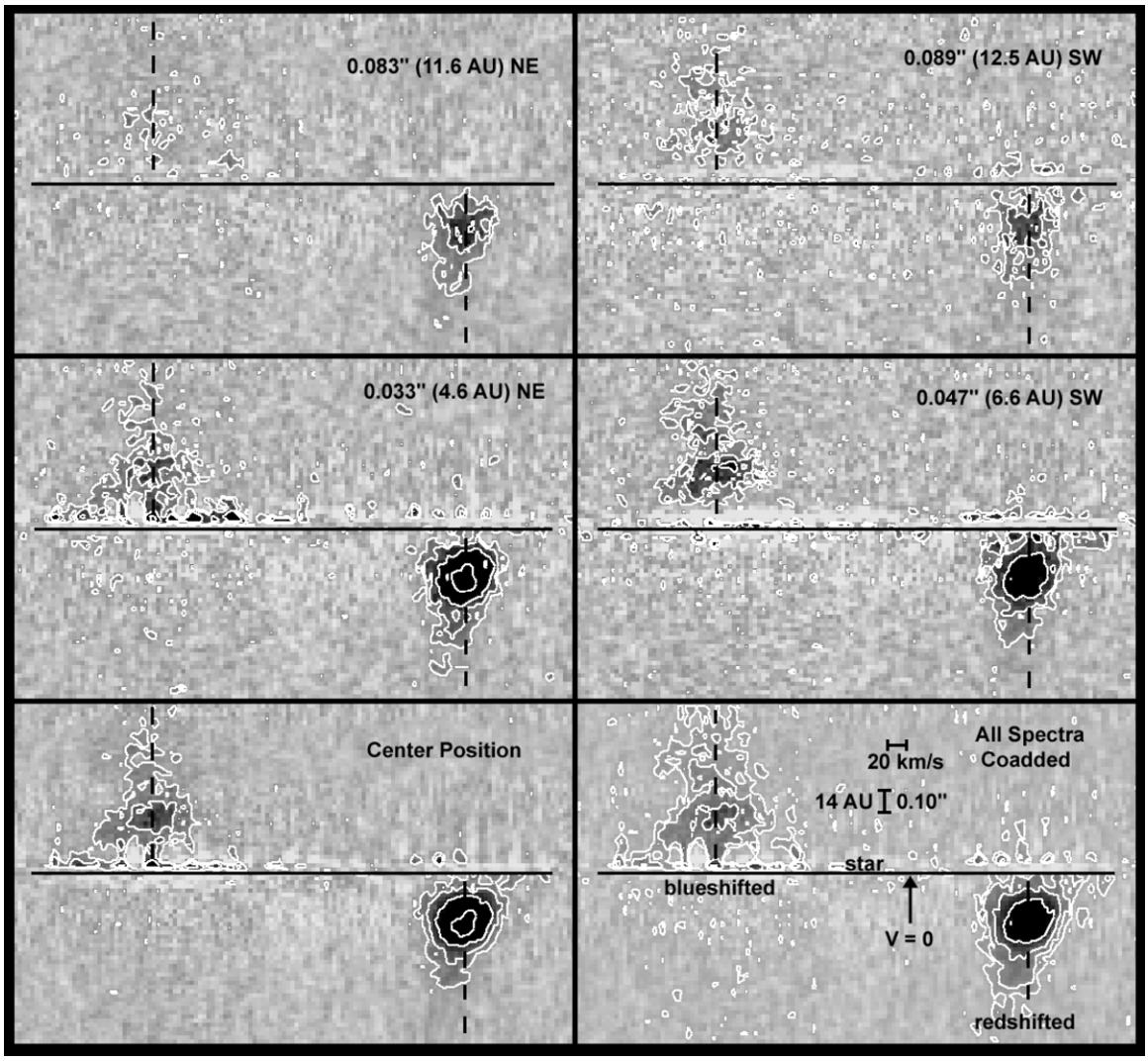

Figure 1. Position–velocity diagrams of the [Fe II] 1.644 μm emission line for five slit positions along the RW Aur jet (P.A. = 125°), co-added as described in the text. The velocity resolution is 20 km s^{-1} and the spatial resolution ~0.06 arcsec. Thin horizontal black lines in each frame show the spatial location of the star, and the arrow in the bottom right frame points to zero (heliocentric) velocity. Dashed vertical lines mark the velocities of the blueshifted and redshifted flows. Adjacent contours differ by a factor of two. There are no significant differences in the position–velocity diagrams for the different slit positions, which are sampled at roughly the Nyquist frequency of the instrumental resolution. The redshifted jet is brighter and slower than the blueshifted jet.

model (Matt & Pudritz 2005) emanates from latitudes between the base of the accretion column and the rotational pole. In each case, the winds are accretion-powered and the models can be "cold" or "warm" depending on whether there is added thermal energy.

Ideally, we would like to use the position–velocity diagrams in Figure 1 to test models of outflows directly. However, to do so requires that models accurately predict radiation from the [Fe II] 1.644 μm line, which in turn requires that the models incorporate all the important heating and cooling processes in their calculations and can predict the flux in this emission line. This is a tall order for any model, because time-variable phenomena such as internal velocity variability and magnetic reconnection appear to dominate the heating in jets within a few hundred AU of the source. For example, recent *HST* observations of the physical conditions in the HH 30 jet show that it emerges mostly neutral, becomes ionized several tens of AU from the source and bright knots, and then moves downstream in the flow (Hartigan & Morse 2007). In RW Aur, there is a large velocity difference between the redshifted and blueshifted jets, with the redshifted jet the brighter of the two. Steady-state, axisymmetric models cannot account for any of these phenomena, which ultimately determine how bright lines appear in position–velocity diagrams. Reconnection geometries in stellar jets depend upon whether the magnetic axis of the disk aligns with that of the star (Ferreira et al. 2006), but detailed calculations of the position–velocities produced by this type of heating are lacking.

Hence, the most robust comparison we can make at present with model position–velocity diagrams is with the velocity extent of the line profile at various places along the jet. This comparison is not without flaws, because if the line does not emit in a particular part of the flow, as might occur if the gas was too cold there or had a different ionization state than the line of interest, then the line profile will not sample the kinematics of that region. In the case of the RW Aur jet, the gas is unlikely to be Fe I, which is easily ionized, or more ionized than Fe II because no other high ionization lines like [O III] exist close to the star. However, the near-IR [Fe II] lines begin to become collisionally quenched when electron densities like those in the jet close to

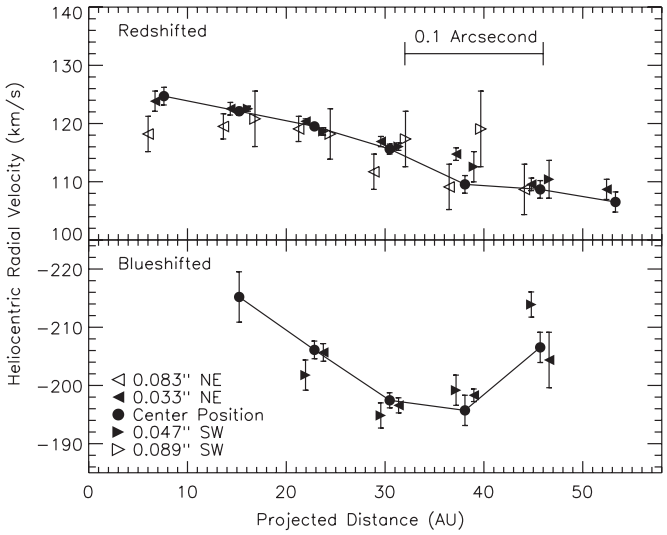

Figure 2. Radial velocities of the [Fe II] 1.644 μm emission for the redshifted and blueshifted parts of the flow. Points taken at the same projected distance for the different slits are offset from one another slightly to avoid confusion. Scatter of values obtained from each 5-minute exposure produces the 1σ error bars. Both the redshifted and blueshifted parts of the flow slow down as the jet emerges from the source. There are no significant differences in the radial velocities observed in the different slit positions.

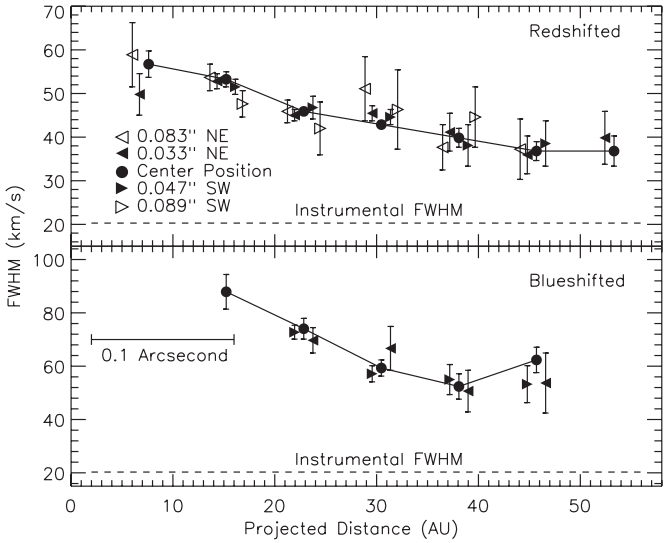

Figure 3. Same as Figure 2 but for the FWHM of the [Fe II] 1.644 μm line profiles. The emission line widths are resolved for all points in the figure, and decrease monotonically with distance from the star.

the source ($\gtrsim 10^4$ cm^{-3}) are reached, and the emission will also decline if the gas cools below a few thousand Kelvin.

Both the redshifted and blueshifted jets have similar appearances in the position–velocity diagram, in that the line profile is wider near the source and narrows with distance. This general behavior occurs in all MHD launching scenarios as the jet becomes collimated, though, as expected, none of the models reproduce the bright knot located about 30 AU from the source on both sides of the flow. One potential interesting constraint from Figure 1 is that no blueshifted emission occurs on the redshifted side of the jet, and no redshifted emission exists on the blueshifted side. This is in conflict with at least one X-wind model (Shang et al. 1998; Pyo et al. 2006), where a wide opening angle near the source produces a large radial velocity dispersion. However, this objection disappears if the jet is simply heated at

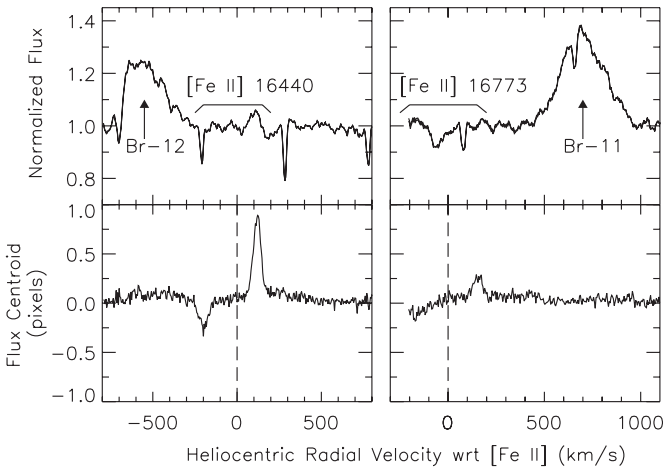

Figure 4. Spectroastrometry of two [Fe II] lines and two Brackett lines. Top: stellar spectrum. The [Fe II] lines at 1.644 μm and 1.677 μm (extent of each line profile indicated by a horizontal bracket) are overwhelmed by the stellar flux. Bottom: spatial position of the flux centroid relative to that of the star. Both Fe lines show clear signatures of bipolar outflow, while the Brackett lines are centered on the stellar position at all velocities. The [Fe II] 1.677 μm line is located at the edge of an order and has an uncertain velocity zero point.

a larger distance once the flow becomes more collimated. The X-wind model has a relatively narrow line width like that observed, but a disk wind can also produce similar line widths, depending on the model parameters (e.g., Pesenti et al. 2004).

As noted by previous authors (e.g., Woitas et al. 2002) the fact that the redshifted jet is visible close to the star implies that the circumstellar disk does not block that portion of the flow. Our spectra trace the redshifted jet to within ~10 AU from the star, so using the known inclination $i = 46°$ for RW Aur (López-Martín et al. 2003), any opaque disk cannot extend beyond ~15 AU from the star. This constraint does not seem particularly surprising, especially since RW Aur is a known binary and the companion could play a role in truncating the outer disk of the primary through dynamical interactions (e.g., Bate 2009).

As noted above, both the redshifted and blueshifted flows have what appears to be a bright knot at about 30 AU from the source (Figure 1). Without time-resolved observations we cannot determine if these features are stationary, or, as typically seen in other flows (e.g., HH 30; Hartigan & Morse 2007), move with the jet. Some of the decline of [Fe II] flux close to the source on the redshifted side may be caused by the disk blocking our view. The knots are not accompanied by a sudden increase in line width, as one would expect for a strong bow shock, but these features could still represent shock waves if the shocks were planar because the curved nature of bow shocks is what produces large line widths. It is worth noting that this close to the source the magnetic field strength may be large enough to significantly inhibit shock formation from variable flow velocities (Hartigan et al. 2007), so the jet may be heated by other mechanisms such as magnetic waves or ambipolar diffusion at tens of AU from the star.

We can use the observed deconvolved line widths to infer something about the flow geometry, assuming radial flow (rotation signatures are at most a few km s^{-1}, and thermal broadening for Fe is also of this order). The ratio of the line width to the jet velocity is an easy dimensionless quantity to measure that depends on the flow geometry. The velocity along the axis of the jet is $V_{\rm jet} = V_{\rm rad}/\cos(i)$, where $V_{\rm rad}$ is the observed radial velocity. The line width along a slice through the axis of

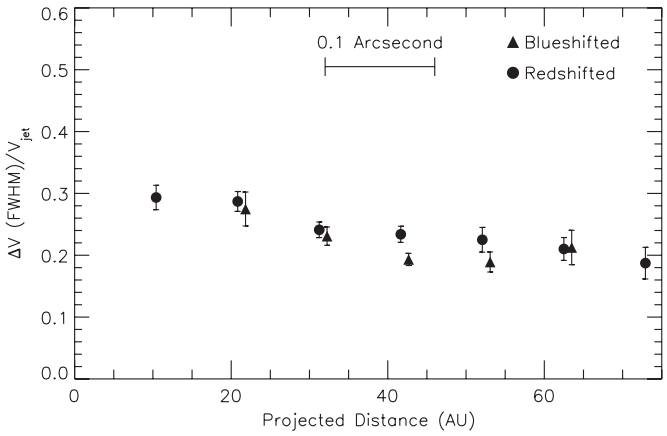

Figure 5. Ratio of the FWHM emission line width of [Fe II] 1.644 μm, corrected for instrumental broadening, to the jet velocity inferred from the radial velocities in Figure 2 and the known inclination angle of the flow. Points and error bars for both the redshifted and blueshifted jets derive from the on-axis values in Figures 2 and 3. The expected ratio for radial flow with an opening angle of 4° is ~ 0.05, so an extra source of line broadening is present in these flows. The redshifted and blueshifted points are offset from one another slightly in distance for clarity.

the jet caused by streamlines that diverge at a full opening angle of δi is simply $\Delta V = V_{\rm jet} \sin(i)\, \delta i$ so that $\Delta V/V_{\rm jet} = \sin(i)\, \delta i$. For RW Aur, $i = 46°$, $\sin(i) \sim 0.7$ and $\delta i \sim 4°$ so that $\Delta V/V_{\rm jet} \sim 0.05$. Figure 5 shows that the observed value of $\Delta V/V_{\rm jet}$ (corrected for instrumental resolution) for both the redshifted and blueshifted portion of the flow is much larger, ~ 0.25. Hence, the large line width in the jet is dominated by different velocities within the slit and not by projection effects of an expanding radial flow with a single velocity. As noted above, the lack of correlation between intensity and line width suggests bow shocks play a minor role in altering the line width.

In the above calculation we have assumed 4° as the opening angle, as observed by Dougados et al. (2000) at distances down to 30 AU from the source, about the location of peak redshifted and blueshifted emission in Figure 1. At closer distances, a larger opening angle would increase the line width for a radial flow. However, Figure 1 shows that the line width increases only about 10% between 30 AU and ~10 AU, where the emission becomes lost in the stellar profile, so the effect of a larger opening angle on the line width between 30 AU and 10 AU appears to be negligible. This is not surprising, as there is no evidence for a larger opening angle in this distance range for other YSO jets that have been observed with STIS (Hartigan et al. 2004).

Because the observations were taken with such a narrow slit, and no emission was observed away from the axis of the flow, the line emission we detect originates from ~14 AU of the axis. According to Figure 5, within this volume the velocity of the [Fe II] emitting gas must change by ~25%. In a disk wind model, the velocity would need to drop off quickly enough off-axis to produce this spread in line width. Alternatively, if the jet is heated in some way by magnetic waves, then the line width should be on the order of the Alfvén speed in the jet. A density of 10^5 cm^{-3} and a line width of 70 km s^{-1} implies a field of ~10 mG if the broadening is purely magnetic. The Alfvénic Mach number of the flow tens of AU from the star would be $V_{\rm jet}/\Delta V \sim 4$.

Figure 5 shows two other interesting aspects of the flow. First, despite the large radial velocity differences between the redshifted and blueshifted jets, the ratio $\Delta V/V_{\rm jet}$ is remarkably similar between the two sides of the flow. Second, there is a subtle but significant trend that this ratio decreases with distance from the star. This decrease occurs because the line width drops more rapidly with distance (Figure 3) than the radial velocities do (Figure 2). In the context of pure magnetic heating, this trend would imply a gradual increase of the magnetosonic Mach number with distance, as one would expect if reconnection or ambipolar diffusion were responsible for heating the jet.

5. SUMMARY

Our Keck spectra of the RW Aur jet are a significant improvement in both spatial and spectral resolution over previous studies of any stellar jet. The jet was unresolved perpendicular to the flow, but the new spectra provide valuable information about the kinematics of the jet to within 10 AU of the source. We confirm several features reported previously, including the velocity asymmetry and bright redshifted flow close to the source. Our observations clearly show larger line widths close to the source for both the blueshifted and redshifted sides of the flow. The ratio of the line width to the jet velocity is about 0.25 for both sides of the flow, a factor of 5 greater than should occur from projection effects in a radial flow. The observed line widths could arise from a layered velocity structure in the jet or from magnetic waves. Spectroastrometry shows no evidence for outflow in the upper Brackett lines.

The Keck spectra illustrate what should become possible as instrumentation on large telescopes continues to improve. Ideally, one would like to have the same or better spectral and spatial resolution as these observations but with a system sensitive enough to detect emission away from the axis of the flow in order to address issues such as rotation and to better quantify the dynamics of the flow. Time-resolved observations are also crucial for determining if the observed knots are stationary or move outward with the jet. If AO systems could be made to work in the optical where emission lines are bright and diagnostics are plentiful we could also learn a great deal about how jets are heated as they emerge from their disks.

P.H. was supported by NASA Origins grant NNG05GH97G during the course of this work. We thank Suzan Edwards for her comments on a draft of this paper.

REFERENCES

Alencar, S., Basri, G., Hartmann, L., & Calvet, N. 2005, A&A, 440, 595
Bate, M. 2009, MNRAS, 392, 590
Blandford, R., & Payne, D. 1982, MNRAS, 199, 883
Cabrit, S., Codella, C., Gueth, F., Nisini, B., Gusdorf, A., Dougados, C., & Bacciotti, F. 2007, A&A, 468, L29
Cabrit, S., Pety, J., Pesenti, N., & Dougados, C. 2005, A&A, 452, 897
Cai, M., Shang, H., Lin, H.-H., & Shu, F. 2008, ApJ, 672, 489
Ceraski, W. 1906, Astron. Nachr., 170, 339
Cerqueira, A. H., Velazquez, P. F., Raga, A. C., Vasconcelos, M. J., & de Colle, F. 2006, A&A, 448, 231
Codella, C., Cabrit, S., Gueth, F., Cesaroni, R., Bacciotti, F., Lefloch, B., & McCaughrean, M. 2007, A&A, 462, L53
Coffey, D., Bacciotti, F., Woitas, J., Ray, T., & Eislöffel, J. 2004, ApJ, 604, 758
Davis, C., Whelan, E., Ray, T., & Chrysostomou, A. 2003, A&A, 397, 693
Dougados, C., Cabrit, S., Lavalley, C., & Menard, F. 2000, A&A, 357, L61
Ferreira, J., Dougados, C., & Cabrit, S. 2006, A&A, 453, 785
Gomez de Castro, A., & Verdugo, E. 2003, ApJ, 597, 443
Hamaan, F. 1994, ApJS, 93, 485
Hartigan, P., Edwards, S., & Pierson, R. 2004, ApJ, 609, 261
Hartigan, P., Frank, A., Varniere, P., & Blackman, E. 2007, ApJ, 661, 910
Hartigan, P., Kenyon, S., Hartmann, L., Strom, S., Edwards, S., Welty, A., & Stauffer, J. 1991, ApJ, 382, 617

Hartigan, P., & Morse, J. 2007, ApJ, 660, 426
Hartmann, L., Hewett, R., Stahler, S., & Mathieu, R. 1986, ApJ, 309, 275
Hirth, G., Mundt, R., Solf, J., & Ray, T. 1994, ApJ, 427, L99
Hornstein, S., Ghez, A., Tanner, A., Morris, M., Becklin, E., & Wizinowich, P. 2002, ApJ, 577, L9
Joy, A. 1945, ApJ, 102, 168
Königl, A., & Pudritz, R. 2000, in Protostars and Planets IV, ed. V. Mannings, A. Boss, & S. Russell (Tucson, AZ: Univ. Arizona Press), 759
López-Martín, L., Cabrit, S., & Dougados, C. 2003, A&A, 405, L1
Matt, S., & Pudritz, R. 2005, ApJ, 632, L135
McGroarty, F., & Ray, T. 2004, A&A, 420, 975
Pesenti, N., Dougados, C., Cabrit, S., Ferreira, J., Casse, F., Garcia, P., & O'Brien, D. 2004, A&A, 416, L9
Petrov, P., Gahm, G., Gameiro, J., Duemmler, R., Ilyin, I., Laakkonen, T., Lago, M. T. V. T., & Tuominen, I. 2001, A&A, 369, 993
Pyo, T., et al. 2006, ApJ, 649, 836
Ray, T., Dougados, C., Bacciotti, F., Eislöffel, J., & Chrysostomou, A. 2006, in Protostars and Planets V, ed. B. Reipurth, D. Jewitt, & K. Keil (Tucson, AZ: Univ. Arizona Press), 231
Ray, T., Muxlow, T. W. B., Axon, D. J., Brown, A., Corcoran, D., Dyson, J., & Mundt, R. 1997, Nature, 385, 415
Rousselot, P., Lidman, C., Cuby, J.-G., Moreels, G., & Monnet, G. 1999, A&A, 354, 1134
Shang, H., Glassgold, A., Shu, F., & Lizano, S. 2002, ApJ, 564, 853
Shang, H., Shu, F., & Glassgold, A. 1998, ApJ, 493, L91
Stout-Batalha, N., Batalha, C., & Basri, G. 2000, ApJ, 532, 474
Whelan, E., Ray, T., & Davis, C. 2004, A&A, 417, 247
White, R., & Ghez, A. 2001, ApJ, 556, 265
Woitas, J., Bacciotti, F., Ray, T., Marconi, A., Coffey, D., & Eislöffel, J. 2005, A&A, 432, 149
Woitas, J., Ray, T., Bacciotti, F., Davis, C., & Eislöffel, J. 2002, ApJ, 580, 336